Draft version January 18, 2016
Preprint typeset using LaTeX style emulateapj v. 01/23/15

THE M33 SYNOPTIC STELLAR SURVEY. II. MIRA VARIABLES

XIAMI[1,*], XIAOYU[1]

Draft version January 18, 2016

ABSTRACT

We have applied the newly developed semi-parametric periodogrom (Citation Coming Soon) on M33 optical observation to search for Miras. We developed M33 data specific models to calculate the probabilities of being Mira for all possible targets. The training data set was constructed by simulating the M33 Mira light curves with known periods and non-Mira light curves in order to train our models. We found XXX Mira candiates, with a XX% discovery rate and XX% purity, which are estimated from the training data set. We tentatively classified the Oxygen-rich and Carbon-rich Miras and give their Period-Luminosity relations.

1. INTRODUCTION

Mira variable stars (Miras) belong to one type of long period variables which is commonly, and empirically, defined as periodic variables with V-band varition greater than 2.5 mag. The pulsating periods of Miras typically range from 100 days to 700 days, but extreme cases can reach beyond 1500 days. They are involved medium or low mass stars at the asymptotic giant branch (Feast 2009).

Thousands of Miras have been identified in the directions of the Milky Way bulge and Magellanic Clouds by the Optical Gravitational Lensing Experiment [Udalski et al. (1992); hereafter OGLE] and MACHO project (Alcock et al. 1993). The Mira light curves obtained by these projects are usually charactered by long time span, full phase coverage, and hundreds of epochs. The Mira light curves are not strictly periodic, but show long-term variations in the mean magnitude and cycle-to-cycle variations. The curve shape for different Miras also varies. Some examples of the light curve variation were described in Huemmerich & Bernhard (2012).

The Mira Period-Luminosity relation (P-L relation) was initially suggested by Gerasimovic (1928). Recent sudies (Glass & Evans 2003) have shown this relation exhibits small scatter at K ($\sigma\sim$0.13 mag), which can be used as distance indicator. The near-infrared Mira P-L relations in Large Magellanic Cloud (LMC), Small Magellanic Cloud, and the Galactic bulge have been explored by Soszyński et al. (2009), Soszyński et al. (2011), and Soszyński et al. (2013) respectively. However, extragalactic Mira P-L relations have not yet been calibrated. Bloom (2013) have proposed a dedicated Mira search in megamaser galaxy NGC 4258 to obtain the infrared Mira P-L relations. In the near future, the LSST project will cover dozens of nearby galaxies where Mira P-L relations can be obtained (LSST Science Collaboration et al. 2009).

In this paper, we conducted a Mira search in M33 using the DIRECT and its follow-up observations [Kaluzny et al. (1998); Pellerin & Macri (2011); hereafter M33 observations]. Although the observational baseline is up to nine years, the number of observations and data quality are significantly lower than those of the OGLE and MACHO projects. At low cadence, the non-periodic variation components of the Mira light curves obstruct period detection. To address this problem, we adopted a semi-parameteric periodogram (Citation Coming Soon) to search for Miras and their periods. This periodogram, which is designed for low-cadence Mira observations, has a Gaussian process component to account for the deviations from exact periodicity, and gives better performances than Lomb-Scargle (Lomb 1976; Scargle 1982) periodogram for M33 observations.

To help identify Miras among other type of stars, we carried out a comprehensive simulation and built classification models using machine learning methods. We extracted XXX features from simulated light curves and their frequency spectra to train the models, then applied the models on the M33 observations to classify Miras. We obtained XXX Mira candidates in M33 with a XX% misclassification rate.

This paper is organized as follows. Section 2 introduces the observations of M33. In Section 3 we report the methods of simulating M33 observations with prior knowledge of light curve classes and periods if they are Miras. Section 4 describes the models which were used to identify Miras and estimate their periods. Section 5 gives the results on real M33 observations.

2. OBSERVATIONS AND PHOTOMETRY OF M33

The detailed descriptions of observations and photometry procedures can be found in the first paper of the series (Pellerin & Macri 2011). Here we briefly summarize them.

Almost the entire disk of M33, which spans approximately half square degree in the sky (Roberts 1895), was observed by the DIRECT project and follow-up observations. The original DIRECT project used the Fred L. Whipple Observatory 1.2m telescope and the Michigan-Darmouth-MIT 1.3m telescope to observe M33 during 1996 September to 1999 Novemeber. Addtional observations was obtained at the Wisconsin-Indiana-Yale-NOAO Observatory 3.5m telescope between 2002 August to 2006 August. In this paper we refer them collectively as M33 observations. We only used the I-band data to search for Miras. The number of I-band observations for individual objects is shown in Figure 1. It is common that there is more than one observations in one night, and as a result the median number of nights with observations

[1] DAHAI
[*] Corresponding author, HUPO@JIANGHE.edu

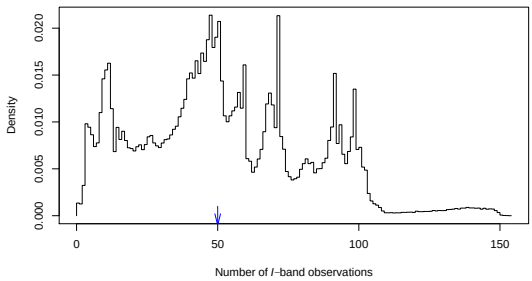

FIG. 1.— The distribution of number of I-band observations for the objects in M33. Objects without detection in certain frames do not count as observations. The blue arrow indicates the median number of observations.

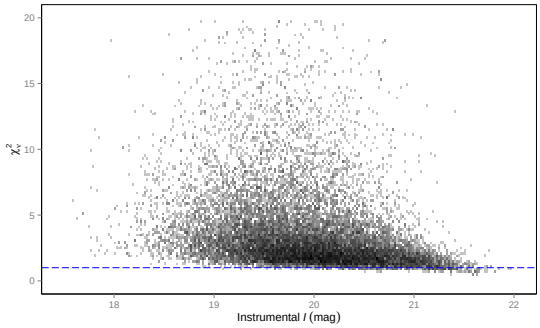

FIG. 2.— χ^2_ν as a function of instrumental I-band magnitude for one field. The depth of color is in log scale of number of stars in each pixel. The blue dashed line indicates the position of $\chi^2_\nu = 1$.

is around 30. The observations consists of 29 fields, and different fields have different distributions of number of observations.

We used the photometry products from Pellerin & Macri (2011). They performed PSF photometry using the DAOPHOT, ALLSTAR, and ALLFRAME (Stetson 1987, 1994), and carried out photometric calibration based on Massey et al. (2006). We used the I-band light curves with Stetson's variability index $J > 0.75$ (Stetson 1996) to carry out Mira search.

3. SIMULATION OF M33 OBSERVATIONS

To build models for searching Miras from the M33 observations, we simulated Mira and Non-Mira light curves as training data. The simulated light curve includes Miras, constant stars, and semiregular variable stars (SRVs). Upon the simulated light curves, we calculated the variability index and kept those with $J > 0.75$. The number of light curves was chosen to match real observations, other properties such as sampling patterns and measurement uncertainties were also derived from the M33 observations. Below we describe the simulations of different kind of light curves.

3.1. *Mira light curves*

We simulated 5000 Mira light curves by applying the M33 sampling patterns and noise levels to LMC Mira light curves from the OGLE observations. The detailed description of simulation method can be found in (Citation Coming Soon), and here we briefly describe the method we used.

We used the model from (Citation Coming Soon) to generate template Mira light curves. The magnitudes of the templates were shifted by 6.2 mag to account for the distance difference between LMC and M33. To simulate a Mira light curve, we randomly selected a sampling pattern from the M33 observations and shifted by some amount to match the baseline of OGLE observations, then selected a template randomly but with weightss from completeness functions of M33 observations, which are derived empirically for three ranges of color.

The noise levels were derived for individual images of M33 observations. We fit the relation between magnitude uncertainties σ and magnitude m with the following empirical function

$$\sigma(t_i, f_k) = a(t_i, f_k)^{[m-b(t_i,f_k)]} + c(t_i, f_k)\,, \qquad (1)$$

where a, b, and c are free parameters and varies with time t_i and field f_k. We then calculated the uncertainties for simulated Mira light curves based on these relations, and added Gaussian noise to their magnitudes with standard deviations at $\sigma(t_i, f_k)$.

3.2. *Constant star light curves*

We simulated $\sim 5 \times 10^5$ light curves for constant stars, which matches the number of observed stars in M33. For the M33 observations, the magnitude uncertainties reported by the photometry software were sometimes either under-estimated or over-estimated. Since both the J index and the Mira periodogram utilize the the value of magnitude uncertainties, we took the inaccuracy of reported magnitude uncertainties into account for the simulated light curves. For constant stars the inaccuracy of uncertainties can be described by

$$\chi^2_\nu = \frac{1}{\sqrt{n-1}} \sum_{i=1}^{n} \frac{(m_i - \bar{m})^2}{\sigma_i^2}\,, \qquad (2)$$

where n is the number of observations. Figure 2 shows the distribution of χ^2_ν as a function of magnitude for all stars in one field of the M33 observations.

For each star in the M33 observations, we calculated χ^2_ν by assuming that it is a constant star. A sampling pattern was then randomly selected from the true light curves in the same field, and the "reported uncertainty" of each epoch was derived based on Equation 1 individually. Finally the simulated magnitude of each epoch was sampled the normal distribution

$$m = \mathcal{N}(m_0, \sqrt{\chi^2_\nu} \cdot \sigma)\,, \qquad (3)$$

where m_0 is the magnitude of that star. The simulated magnitude uncertainty was still set to σ from Equation 1. In this way the simulated light curves give the same inaccuracy of magnitude uncertainties as the real light curves. An example of simulated constant star light curve is given in Figure 3.

We note that the assumption of all stars in the M33 observations being constant stars is not correct generally, because there should be some variable stars among them. But the amount of variable stars are small relative to the entire sample of stars. An advantage of this method is that stars of bad photometry results, which may be due to bad pixels or frame edges, were also simulated.

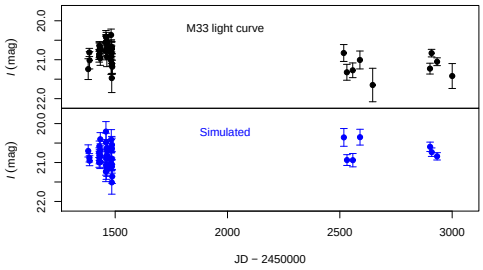

FIG. 3.— An example of simulated constant star light curve (lower) and its corresponding real light curve (upper). The errorbars for the simulated light curve indicate the "reported uncertainties", which were rescaled before adding noise the light curve.

3.3. *SRV light curves*

SRVs share some similarities with Miras, and thus may increase the misclassification rate for M33 Mira search. Although SRV light curves are more chaotic and non-periodic than Mira light curves, the magnitudes and the amount of magnitude variations for some SRVs are compariable to Miras. Due to the sparse nature of the M33 observations, some SRVs in M33 may be misclassified as Miras. To improve the ability of discriminating SRVs and Miras, we included simulated SRV light curves in the training data. This would also help us to assess the misclassification rate.

We simulated 5000 SRV light curves with the approach similar to the simulation of Mira light curves. The only difference is that we smooth splined the LMC SRV light curves to obtain template SRV light curves.

4. MODELS

$1 - 5 light curves - - > Stetson's J > 0.75 - - > Simulated dataset$

Apply GP on simulated data set

4.1. *model 1*

Regression (ridge, lasso ?)

4.2. *model 2*

Beyes, cart, svm?

4.3. *model 3*

Deep learning?

5. RESULTS

REFERENCES

Alcock, C., Allsman, R. A., Axelrod, T. S., et al. 1993, in Astronomical Society of the Pacific Conference Series, Vol. 43, Sky Surveys. Protostars to Protogalaxies, ed. B. T. Soifer, 291
Bloom, J. 2013, Absolute Calibration of the Extragalactic Mira Period-Luminosity Relation, HST Proposal
Feast, M. W. 2009, in AGB Stars and Related Phenomena, ed. T. Ueta, N. Matsunaga, & Y. Ita, 48
Gerasimovic, B. P. 1928, Proceedings of the National Academy of Science, 14, 963
Glass, I. S., & Evans, T. L. 2003, MNRAS, 343, 67
Huemmerich, S., & Bernhard, K. 2012, Open European Journal on Variable Stars, 149, 1
Kaluzny, J., Stanek, K. Z., Krockenberger, M., et al. 1998, AJ, 115, 1016
Lomb, N. R. 1976, Ap&SS, 39, 447
LSST Science Collaboration, Abell, P. A., Allison, J., et al. 2009, ArXiv e-prints, arXiv:0912.0201
Maercker, M., Vlemmings, W. H. T., Brunner, M., et al. 2015, ArXiv e-prints, arXiv:1512.01350
Massey, P., Olsen, K. A. G., Hodge, P. W., et al. 2006, AJ, 131, 2478
Pellerin, A., & Macri, L. M. 2011, ApJS, 193, 26
Roberts, I. 1895, MNRAS, 56, 70
Scargle, J. D. 1982, ApJ, 263, 835
Soszyński, I., Udalski, A., Szymański, M. K., et al. 2009, Acta Astron., 59, 239
—. 2011, Acta Astron., 61, 217
—. 2013, Acta Astron., 63, 21
Stetson, P. B. 1987, PASP, 99, 191
—. 1994, PASP, 106, 250
—. 1996, PASP, 108, 851
Udalski, A., Szymanski, M., Kaluzny, J., Kubiak, M., & Mateo, M. 1992, Acta Astron., 42, 253